DOI: 10.1021/ma901623s

Macromolecules
ARTICLE

Structure and Morphology in Highly Oriented Films of Poly(9,9-bis(*n*-octyl)fluorene-2,7-diyl) and Poly(9,9-bis(2-ethylhexyl)fluorene-2,7-diyl) Grown on Friction Transferred Poly(tetrafluoroethylene)

Martin Brinkmann,*,† Nipaphat Charoenthai,‡ Rakchart Traiphol,‡ Phimwipha Piyakulawat,§ Joerg Wlosnewski,§ and Udom Asawapirom§

†*Institut Charles Sadron, CNRS-Université de Strasbourg, 23 rue du loess, BP 84047, 67034 Strasbourg Cedex 2, France,* ‡*Laboratory of Advanced Polymers and Nanomaterials, Department of Chemistry and Center for Innovation in Chemistry, Faculty of Science, Naresuan University, Phitsanulok 65000, Thailand, and* §*National Nanotechnology Center, National Science and Technology Development Agency, Thailand Science Park, Pathumthani 12120, Thailand*

Received July 23, 2009; Revised Manuscript Received August 7, 2009

ABSTRACT: This study focuses on the epitaxial orientation of two polyfluorenes (PF) namely poly-(9,9-bis(n-octyl)fluorene-2,7-diyl) (PFO) and poly(9,9-bis(2-ethylhexyl)fluorene-2,7-diyl) (PF2/6) on friction transferred poly(tetrafluoroethylene). PF2/6 films with a single-crystal like orientation are obtained on PTFE substrates after proper annealing whereas only marginal orientation is observed for PFO films. For both polymers, the crystalline lamellae grow essentially perpendicular to the PTFE chain direction and the epitaxial conditions were determined as $[0\ 0\ 1]_{PF}//[0\ 0\ 1]_{PTFE}$ and $(0\ 1\ 0)_{PF}//(1\ 0\ 0)_{PTFE}$. For PF2/6 samples with different molecular weight distributions, the lamellar thickness tends to increase with increasing average molecular weight of the polymer. The close examination of the selected area electron diffraction (SAED) patterns corresponding to the $[0\ 1\ 0]_{PF26}$ zone supports a 21_4 helical conformation of the PF2/6 chains. A simple structural model based on a trigonal cell with *P*3 space group, $a = b = 1.68$ nm and $c = 16.9$ nm containing a triplet of 21_4 helices accounts well for the main features of the observed electron diffraction pattern. The three 21_4 helices of the triplet show periodic short contacts every fifth monomer along the helix axis, suggesting that the supramolecular assembly of the PF2/6 chains forming the triplet is stabilized by efficient π-stacking between fluorene monomers. The observed difference in orientation of PF2/6 and PFO on PTFE substrates supports an orientation mechanism involving the PTFE macrosteps.

1. Introduction

In the past few decades, semiconducting polymers (SCPs) like regioregular poly(3-alkylthiophene)s, substituted poly(*p*-phenylenevinylene)s and polyfluorenes have become key materials in the preparation of various opto-electronic devices, e.g., organic light emitting diodes (OLEDs), organic solar cells and organic field effect transistors (OFETs). The control of the thin film morphology and structure has been recognized as an essential step toward the optimization of the performances of these electronic and opto-electronic devices.[1−3] However, the crystallizing and/or self-assembling properties of SCPs have not been understood thoroughly so far. In particular, it is of utmost importance to correlate the structure formation to the intimate chemical structure of the polymers.[4] In this perspective, the respective roles of the alkyl side chain organization and the $\pi-\pi$ stacking between the conjugated backbones on the crystallization of hairy-rod polymers e.g. polyfluorenes has to be further clarified. Soluble polyfluorenes like poly(9,9-bis(*n*-octyl)fluorene-2,7-diyl) (PFO) and poly(9,9-bis(2-ethylhexyl)fluorene-2,7-diyl) (PF26) form a unique class of blue-emitting polymers[4,5] of interest for their use in various optoelectronic devices, e.g., polarized light emitting diodes (PLED's)[6,7] or electrically pumped organic lasers.[8] Concerning the structure of polyfluorenes, significant differences are observed upon changing the structure of the alkyl side chains which seems to impact the conformation of the conjugated polyfluorene backbone.[4] In the case of PFO, photophysical studies have evidenced two different backbone conformations, namely α and β, whose occurrences depend closely on the preparation method of the samples, e.g., annealing or solvent vapor exposure.[9−14] In their liquid crystalline forms, PFO and PF2/6 can be readily oriented on rubbed polyimide substrates,[15,16] by a friction transfer method[17] or by directional epitaxial crystallization (DEC) in 1,3,5-trichlorobenzene (TCB).[18] Shear-orientation was also used to prepare highly oriented thin films suitable for structural investigations.[19] This aligning ability of PFs has been successfully used to achieve anisotropic charge transport as well as polarized electroluminescence and/or photoluminescence.[16,20]

In the present study, we have focused on the possibility to orient PFO and PF2/6 on friction transferred poly(tetrafluoroethylene) (PTFE) substrates.[21] The friction transfer of PTFE on a substrate of glass or a silicon wafer at 300 °C results in the deposition of a very thin PTFE film with a single-crystal like orientation so that the polymer chains are oriented in the direction parellel to the friction direction.[21] Such PTFE substrates have been widely used to orient a large palette of conjugated molecular materials (sexithiophene,[22] acenes,[23] phthalocyanines and porphyrins,[24] Alq,[25] *p*-nitroaniline,[26] etc.) and conjugated polymers (polydiacetylenes[27]) yielding films with exceptional levels of orientation. Whereas several studies have been dedicated to oriented PFs films grown on rubbed polyimide substrates,[15,16] no study has been reported in the case of highly oriented poly(tetrafluoroethylene) substrates. The present work

*Corresponding author. E-mail: brinkman@ics.u-strasbg.fr.

 Published on Web 08/25/2009

Table 1. Macromolecular GPC Parameters (M_n, M_w and PDI = M_w/M_n) and Average Lamellar Thicknesses for Edge-on Oriented PF2/6 Lamellae Oriented on PTFE Substrates[a]

sample	M_n (kDa) equiv of PS	M_w (kDa) equiv of PS	PDI = M_w/M_n	lamellar thickness (nm)
S1	43.7	124.7	2.85	124
S2	21.0	45.9	2.2	73
SF1	38.0	147.2	3.87	101
SF2	25.3	41.64	1.64	59

[a] S1 and S2 refer to the unfractionated samples whereas the SF1 and SF2 samples were obtained by fractionation in chloroform and ethyl acetate, respectively.

uncovers important differences in the orientation of PFO and PF2/6 on oriented PTFE substrates. Whereas a very high level of orientation and crystalline order is achieved in the case of PF26, only moderate orientation is observed for PFO. Our study also highlights the impact of the average molecular weight of PF2/6 on the average lamellar thickness. The results of the simulation of the experimental electron diffraction patterns obtained for oriented PF26 films on PTFE confirm that PF26 forms a 21_4 helix in a trigonal unit cell. The higher orientation level observed for oriented PF2/6 films on PTFE is explained in terms of a matching between the PTFE ledge topography and the hexagonal packing of PF2/6 chains.

2. Experimental Section

(2.1). Polymer Samples. Both, PFO and PF2/6 were synthesized using the methods published in the literature.[28,29] Typically, the synthesis of the PF2/6 was accomplished by the Yamamoto-type coupling reaction of 2,7-dibromo-9,9-bis-(2-ethylhexyl)fluorene using bis(1,5-cyclooctadiene)nickel(0) as the catalyst.[29] Different reaction times in the range 2−4 days were used to obtain polymers with different weight-average molecular masses (samples labeled S1 and S2 in Table 1). The raw polymer was extracted in a Soxhlet apparatus with methanol and acetone, respectively, to remove impurities and oligomers. Subsequently, one polymer sample was fractionated by applying the solvent extraction method.[3] Following extraction steps with solvents of an increasing solubility for PF2/6 (ethyl acetate and chloroform) yielded two polymer fractions (samples labeled SF1 and SF2 in Table 1). The resulting polymer fractions were concentrated, precipitated in MeOH/ 2N aqueous HCl (10/1; v/v), collected and dried under vacuum. The ^{1}H NMR analysis of both PF2/6 fractions did not show significant structural differences of the samples.

The various samples were characterized by multiple detector size exclusion chromatography (SEC) using THF (HPLC grade) as the eluent and a PS calibration. The SEC setup consisted of a Shimadzu LC10AD pump, an ERMA ERC3512 online degasser, a WATERS 717+ automatic injector and five 300×7.5 mm^2 PL Gel columns from Polymer Laboratories ($4 \times 10\,\mu$m Mixed-B and one 500 Å) connected in series and a refractive index (RI) detector (Shimadzu RID10A). The weight-average molecular weight obtained from SEC (polstyrene standard) was ca. 104 kDa with a polydispersity index of 2.95 for the PFO sample used herein whereas the macromolecular data of the PF2/6 samples are collected in Table 1.

(2.2). Thin Film Preparation and Analysis. PTFE films were prepared according to the method described elsewhere[21,23] by sliding a PTFE rod at a constant pressure (5 bar) against a glass slide (Corning 2947) held at 250−300 °C. Cleaning of the glass substrates was obtained by (i) sonication in acetone (15 min), (ii) sonication in ethanol (15 min), (iii) mechanical scrubbing with a soft tooth brush using a distilled hellmanex (Hellma Gmbh) solution in deionized water, and (iv) sonication in deionized water (3×). The slides were subsequently dried in a flow of nitrogen. The purpose of the cleaning procedure, especially the mechanical scrubbing, is to remove microparticle that could perturb the friction-transfer of PTFE. The thin films were prepared by either drop-casting a 1 wt % solution in chloroform on PTFE or using the doctor-blade technique with a 4 wt % solution (in chloroform) on the substrates maintained at 65 °C. The thickness of the films determined by AFM was in the range 30−110 nm. Annealing was performed by using a THMS-600 hot stage (Linkam) connected to a TMS-94 temperature controller. Prior to annealing under nitrogen, the chamber of the hot stage was purged several times with the inert gas. Typical annealing procedures were as follows: first the sample was annealed to a temperature above the crystal → liquid crystal transition temperature i.e. 210 °C for PFO and 180 °C for PF2/6. The heating rate was 30 °C/min and the PFO (respectively PF2/6) films were left at 210 °C (respectively 180 °C) temperature for 1 min. This annealing step was followed by a slow cooling to room temperature at a rate of 0.4 °C/min.

For TEM observations, the PF films were coated with a thin amorphous carbon film and the PF/carbon film was removed from the glass substrate by dipping the films into an aqueous HF solution (5 wt %). The PF/carbon layers were subsequently recovered onto TEM copper grids. TEM was performed in bright field, dark field and rotation−tilt configurations on a CM12 Philips microscope equipped with a MVIII CCD camera (Soft Imaging Systems). The surface topography of PF thin films was investigated by atomic force microscopy (AFM) with a Nanoscope III in tapping mode using Si tips (25−50 N/m and 280−365kHz). Image treatments (FFT) were performed by using AnalySIS (Soft Imaging System) and SXM (NIH) softwares.

For the determination of the lamellar thickness distribution, we have used the DF images which underline very clearly the grain boundaries between successive lamellae (see Figures 3 and 4). The contours of the lamellae were first highlighted and then a section profile was plotted in the direction parallel to the PF chains (PTFE chain axis direction), i.e., perpendicular to the PF lamellae. The coordinates of the intersection points between the profile line and the contours of the lamellae were recorded upon moving the profile line in the direction of the PF chains, i.e., perpendicular to the lamellae with steps of 3 pixels. The x-positions of these intersections were subsequently converted to lamellar thicknesses yielding 300−500 data points for the distribution determination after proper binning.

UV−vis−near IR absorption of the thin films (300−900 nm) was measured on a Shimadzu UV-2101PC spectrometer with polarized incident light and spectral resolution of 1 nm. The photoluminescence (PL) was measured on a Jobin Yvon Fluoro-Max4 spectrofluorimeter with a slit width of 1 and 2 nm for excitation and emission respectively. The wavelength of the excitation was fixed at 385 nm and the excitation light was not polarized.

3. Results and Discussion

3.1. Thin Film Morphology and Orientation. The orientation achieved in the as-cast PFs thin films on PTFE is relatively minor. Annealing the PF thin films to 180 °C for PF2/6 and 210 °C for PFO during 1 min, followed by a slow cooling (0.4 °C/min) to room temperature promotes the crystallization and the formation of lamellar crystals. Figure 1 and 2 depict the typical bright field and the electron diffraction patterns for the annealed PFO (M_n = 35 kDa) and PF2/6 (M_n = 43.7 kDa) thin films on PTFE. Let us first focus on the case of PFO. As seen in Figure 1, the TEM BF shows the

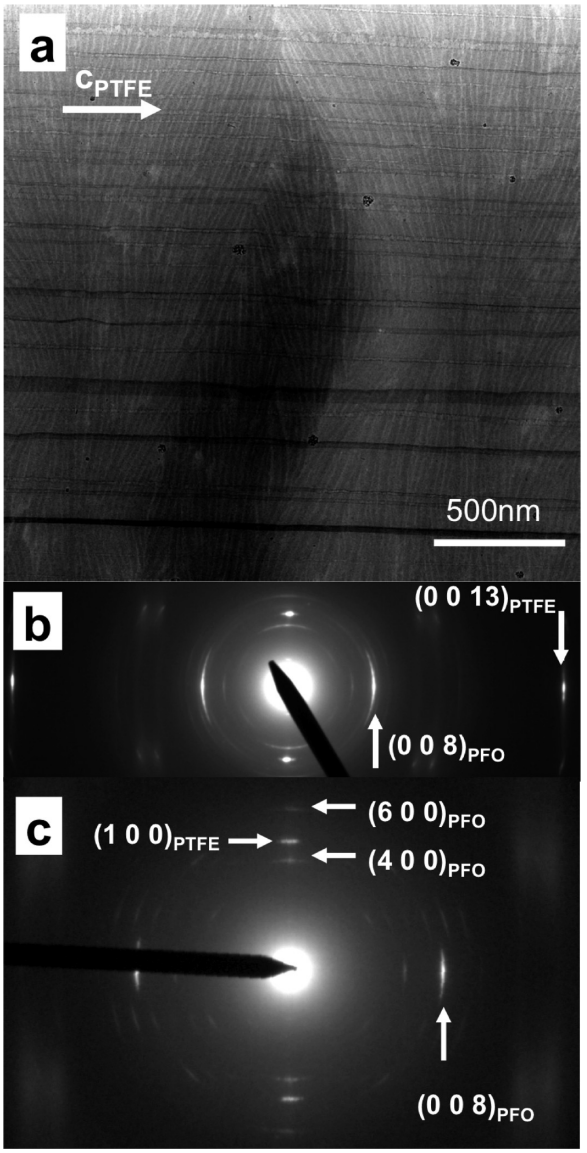

Figure 1. (a) TEM bright field of an oriented PFO thin film on a PTFE substrate. The PFO film was annealed at 210 °C for 1 min and cooled slowly to room temperature at 0.4 °C/min. (b) Electron diffraction pattern in proper relative orientation to the bright field image. (c) Selected area electron diffraction pattern.

lamellar structure similar to that observed for PFO films oriented by directional epitaxial crystallization in TCB.[18] However, in the case of PFO grown on PTFE, the crystalline lamellae exhibit strong in-plane splay and tend to deviate from the perpendicular orientation to the PTFE axis, which suggests a rather poor orienting effect of PTFE on PFO. Overall, the obtained morphology is similar to the axialite structure found for PFO on glass substrate.[13]

In contrast to PFO, the annealed PF2/6 samples on PTFE consist of crystalline lamellae oriented essentially perpendicular to the PTFE chain direction. The difference between the orientation levels of PFO and PF2/6 is further apparent from the ED patterns in Figures 1 and 2. In the case of PFO, a strongly arced reflection at 0.834 nm which corresponds to the monomer repeat period along the PFO chain is observed (in Figure 1, this reflection is indexed as 0 0 8 using the orthorhombic structure of PFO[13,18]). This reflection is oriented in the direction of the (0 0 13) reflection of PTFE

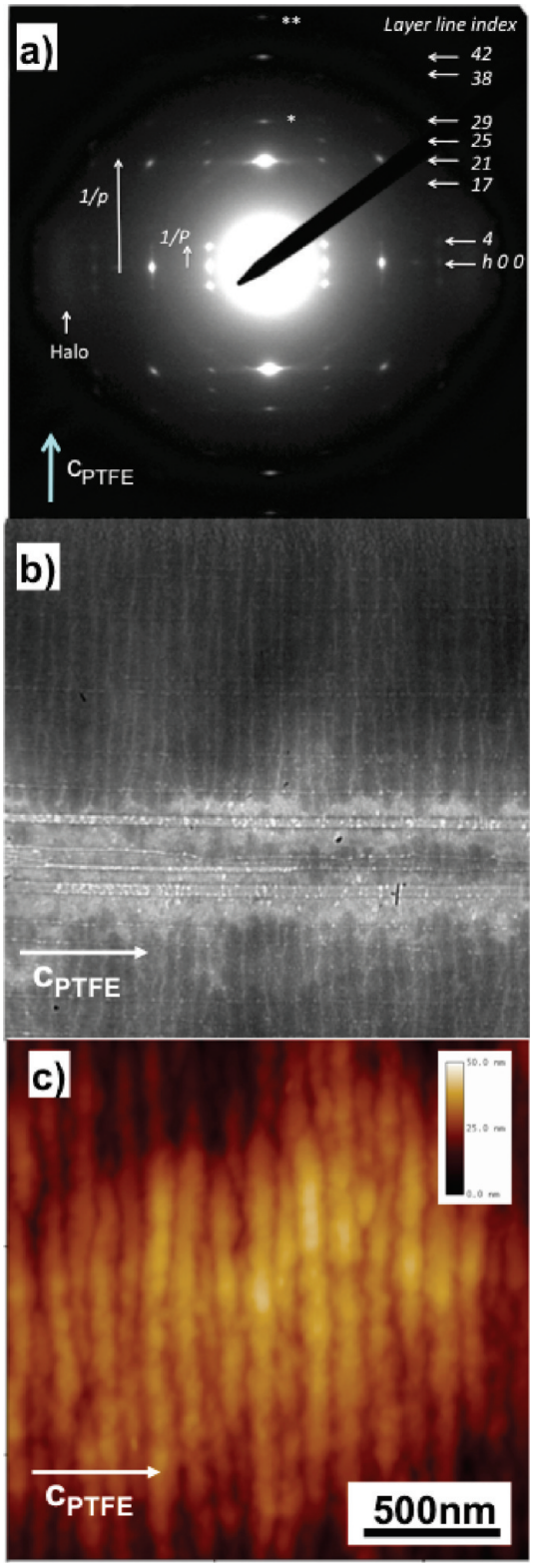

Figure 2. (a) Electron diffraction pattern of a highly oriented PF2/6 thin film (M_n = 43.7 kDa) grown on oriented PTFE substrate after annealing at 180 °C (1 min) and slow cooling to room temperature (0.4 °C/min). The layer lines have been indexed on the basis of a 21_4 helix as discussed in the text. Additional reflections on the meridian have been highlighted by asteriks as well as the position of the diffuse halo. (b) Corresponding TEM bright field micrograph. The PTFE chain axis direction c_{PTFE} is indicated by a white arrow. (c) Topographic AFM image showing the periodic lamellar structure of the PF2/6 thin film.

indicating that the PFO chain direction tends to orient parallel to the PTFE chains. The strong arcing of the reflection reflects the large distribution of in-plane orientations of the PFO crystalline lamellae. On the equator, the ED pattern shows the typical 0 4 0 and the 0 6 0 reflections of the orthorhombic cell of PFO.[13,18] The overall SAED pattern shown in Figure 1c is typical of the [0 1 0] zone and compares very well with that observed for films oriented by epitaxy on TCB[18] or by friction transfer.[17] These observations suggest that PFO chains tend to be oriented parallel to the chains of the PTFE substrate and that the $(0\ 1\ 0)_{PFO}$ plane is the preferential contact plane on PTFE.

As seen in Figure 2, the ED pattern of PF2/6 exhibits remarkably sharp reflections with negligible arcing as compared to PFO. The most intense meridional reflection at $d_{hkl} = 0.806$ nm corresponds to the monomer repeat period along the chain axis of PF2/6; it is indexed as 0 0 21 using the hexagonal structure determined hereafter. The observed monomer repeat period compares very well with that obtained by Knaapila et al. for shear-oriented samples (0.808 nm).[19] This reflection is oriented in the direction of c_{PTFE} indicating that the PF2/6 chains are oriented parallel to the PTFE chains. On the equator, the ED pattern shows exclusively the (h 0 0 reflections) ($h = 1, 2,$ and 3) with $d_{001} = 1.48$ nm. The overall pattern is in close agreement with that obtained in earlier studies for PF2/6 films grown on rubbed polyimide substrates[15] or oriented under shear.[19] However, we observe one major difference, namely, in the case of the PF2/6 films grown on the PTFE substrate, the ED pattern indicates a perfect biaxial orientation; i.e., the crystalline lamellae of PF2/6 grow with a preferential $(0\ 1\ 0)_{PF2/6}$ contact plane on the PTFE substrate. This very high orientation of the PF2/6 films on PTFE is also reflected in the anisotropy of the optical absorption and photoluminescence. In Figure 3, we show the UV−vis absorption and the fluorescence spectra of a representative oriented PF2/6 thin film (ethyl acetate fraction with $M_n = 21$ kDa) on PTFE substrate prior and after thermal annealing at 180 °C. Prior to annealing, the PF2/6 films show some anisotropy in both, absorption and fluorescence. Typically, the dichroic ratio in absorbance at 385 nm (defined as the ratio between the absorbances measured for parallel and perpendicular orientation of the PTFE chain direction vs incident light polarization) increases from 1.8 before annealing to a value in the range 4−5 after annealing. A similar improvement of the film orientation after annealing is evidenced upon thermal annealing by following the evolution of the PL; the dichroic ratio of the PL at 418 nm increases from 1.2 to more than 6 after annealing. More generally, for the various investigated samples, the dichroic ratio of the PL after annealing is found in the range 6 - 8.5. Overall, these values suggest a better orientation of the PF2/6 films on PTFE with respect to films grown on rubbed polyimide substrates for which a dichroic ratio of 3.79 has been reported for the PL of annealed samples.[28]

To summarize, the structural relations at the PFO/PTFE and PF2/6/PTFE interfaces can be writen as:

$$(010)_{PFO}//(010)_{PTFE} \quad \text{and} \quad [001]_{PFO}//[001]_{PTFE} \qquad (1)$$

$$(010)_{PF2/6}//(010)_{PTFE} \quad \text{and} \quad [001]_{PF2/6}//[001]_{PTFE} \qquad (2)$$

Interestingly, on the equator, the ED pattern of PF2/6 exhibits a typical diffuse halo at $d_{hkl} = 0.46$ nm. This distance is reminiscent of the typical interchain distance in polyethylene and suggests the presence of structural disorder in the packing of the branched ethylhexyl side chains. As a matter of fact, the overall ED pattern and the presence of the halo are independent of the molecular weight of the PF2/6 samples investigated herein (see Table 1).

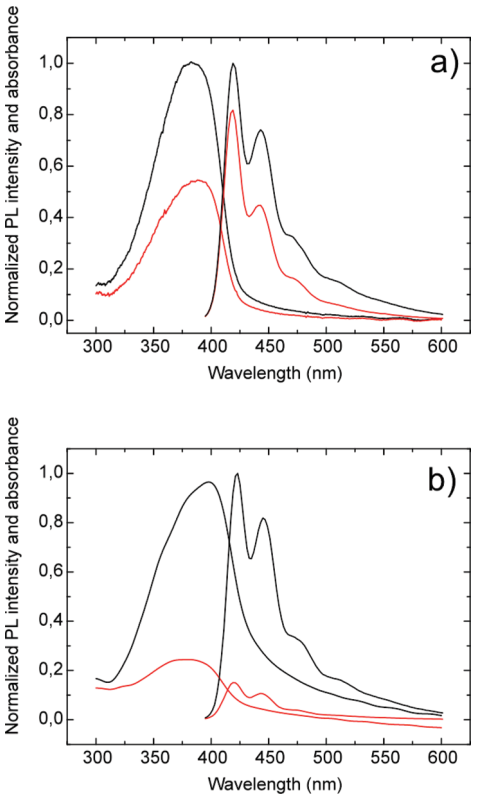

Figure 3. Polarized PL and UV−vis absorption spectra for oriented PF2/6 thin films on PTFE substrates for (a) as-deposited PF2/6 films on PTFE and (b) annealed films (180 °C for 1 min with a slow cooling at 0.4 °C/min). The absorption curves in red (black) correspond to the incident light polarization oriented perpendicular (parallel) to the PTFE chains direction. The PL curves in red (black) correspond to the PL signal measured when the emission is polarized perpendicular (parallel) to the PTFE chain direction.

The comparison of the orientation levels achieved for PF2/6 and PFO on PTFE suggest that the orienting ability of PTFE is sensitive to the structure of the PF polymer chain and hints at the possible existence of an epitaxial orientation mechanism (*vide infra*).

3.2. Dependence of Lamellar Thickness on Macromolecular Parameters. In conjugated polymers like regioregular P3ATs, recent studies on epitaxied thin films have evidenced a lamellar structure whose total periodicity was found to depend on the average M_w of the polymer.[31,32] In the case of PFs, no such study has been proposed so far. The major difference between PFs and P3ATs is the fact that the former crystallize with extended chains due to their higher rigidity (a persistence length of 8.5 nm is reported for PFO) which hinders the possibility of chain folding.[18] The morphology results in epitaxied PFO thin films grown by DEC have shown that the polymer crystallizes with extended chains in the lamellae. It is thus not unexpected to observe some scaling between the lamellar thickness and M_n.

In Figure 4, we depict the lamellar structure in dark field mode for a low-M_n (21 kDa) and a high-M_n sample (43.7 kDa). Both these polymers are also characterized by a high polydispersity index > 2. The DF image was obtained by selecting the 0 0 21 reflection with an objective aperture of 10 μm. In the DF image, the diffracting zones appear bright and the boundaries between successive lamellae as narrow and dark lines. No extended amorphous interlamellar zones are observed as in

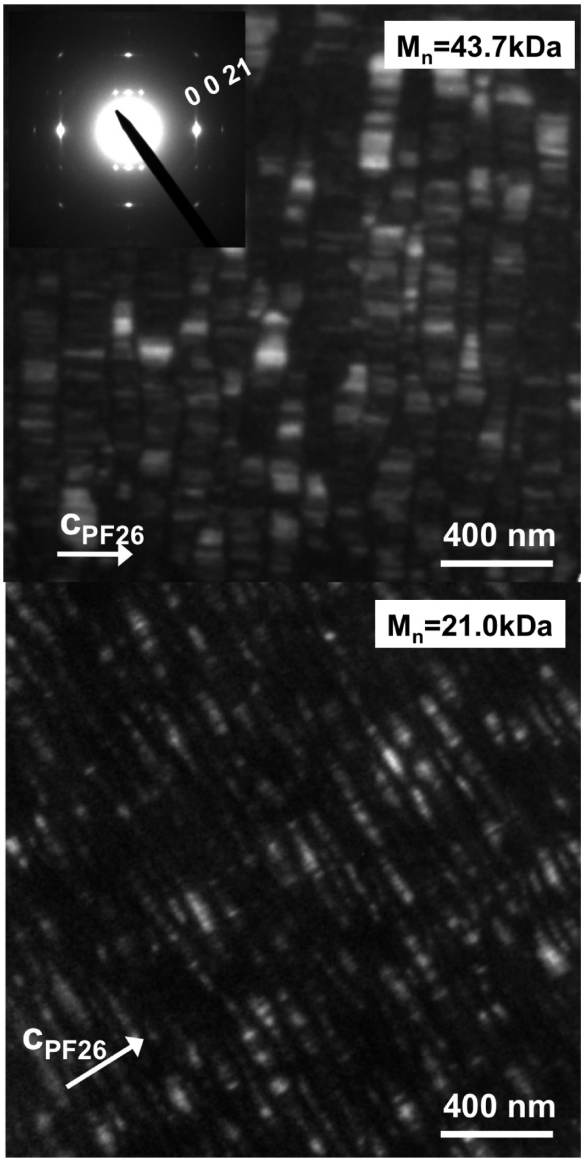

Figure 4. Effect of increasing M_n on the lamellar morphology of oriented PF2/6 thin films on PTFE substrate for two samples with PDI ≥ 2.2 as observed by TEM in the dark field mode selecting the intense 0 0 21 reflection (see the inset for the electron diffraction pattern). The films have been annealed at $T = 180$ °C (1 min) and slowly cooled to room temperature (0.4 °C/min).

the case of P3ATs.[31,32] This observation is in line with our earlier results on the oriented PFO films grown by DEC in TCB and suggest that PF2/6 also crystallizes with extended chains (as opposed to folded chains for regioregular poly(alkylthiophenes)[31,32]). More interestingly, the DF images in Figure 4 show that the average lamellar thickness tends to increase with increasing M_n. Because of strong fluctuations in the lamellar spacings, we resorted to a statistical measurement of the lamellar thickness L_c in the direction parallel to the chain direction, i.e., from one dark grain boundary line to the next one in order to ascertain the qualitative observations gained from the DF images. In Figure 5, we present the distributions of the lamellar thicknesses for the 21 and 43.7 kDa samples (PDI > 2). For the 21 kDa sample, we obtain $L_c = 73$ nm whereas for the 43.7 kDa sample, $L_c = 124$ nm. These results indicate that the lamellar thickness does indeed increase with increasing M_n. A similar increase of average lamellar thickness with M_n is also observed for the

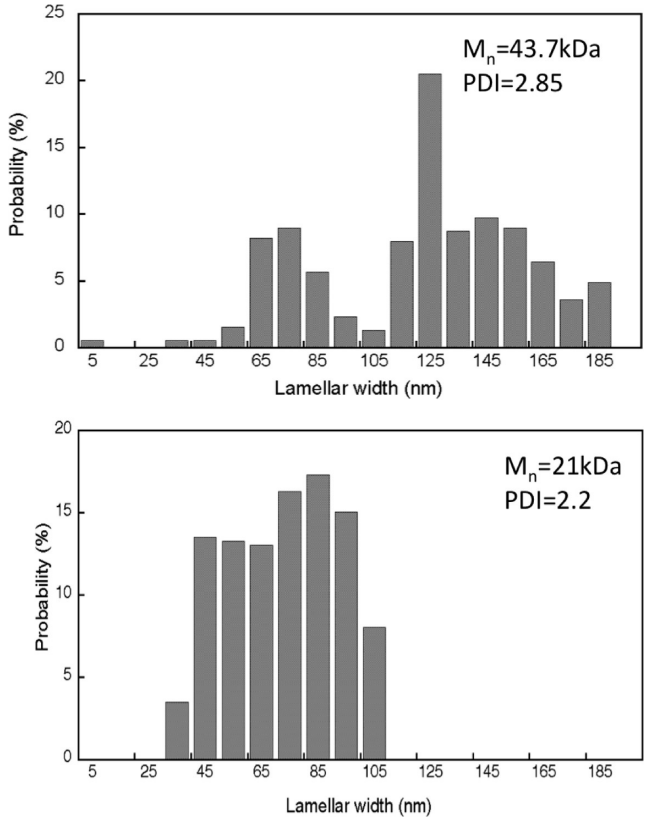

Figure 5. Effect of the average molecular weight in number (M_n) on the distribution of the lamellar thickness obtained from the DF images of oriented PF2/6 thin films on PTFE substrates.

fractionated samples of PF2/6 (see Table 1). As a matter of fact, a direct proportionality between L_c and M_n is however difficult to demonstrate because the values of M_n are signifcantly overestimated by SEC for hairy-rod polymers like PFs. These results suggest that highly oriented and nanostructured PF2/6 thin films could be obtained for polymers with a very narrow chain length distribution. Moreover, the increase of lamellar thickness with M_n suggests that interlamellar grain boundaries (dark lines observed in the DF images) which are detrimental to efficient charge transport could be effectively reduced by increasing the average molecular weight of the polymer.

3.3. Structural Analysis of PF2/6. *3.3.1. Helical Conformation of the Chains*. One key aspect in the determination of the crystal packing of PF2/6 is the intrinsic helicity of the chain. In the case of 2,2′-bifluorene, Blondin et al. have predicted the existence of two low energy conformers having torsion angles of 45° and 135° using *ab initio* calculations.[33] Similarly, in the case of the PF2/6 chain, Tanto et al. have determined the existence of different low-energy conformers with torsion angles of 50°, 135°, and 35° [34] However, these calculations were obtained for isolated chains and it cannot be excluded that the packing of the polymer chains in the crystal with trigonal symmetry results in deviation of the chain conformation from the ideal calculated 5_1 and 5_2 helices. Knaapila et al. first pointed out the possible frustration arising from the packing of 5_1 or 5_2 helices in a crystal with hexagonal symmetry.[19] A close investigation of the diffraction patterns of shear-oriented PF2/6 films indicated a very clear deviation from a 5_1 symmetry as proposed originally by Lieser et al.[15] The latter authors proposed that PF2/6 crystallizes in a trigonal cell with $a = b = 1.67$ nm, $c = 4.04$ nm, $\alpha = \beta = 90°$ and $\gamma = 120°$. However, the lack

of in-plane orientation in the PF2/6 films grown on rubbed polyimide hampered the precise determination of the chain conformation. In a recent study, Knaapila et al. managed to obtain very high levels of orientation in shear-oriented PF2/6 films whose X-ray diffraction patterns enabled the reinvestigation of the helical conformation of PF2/6.[19] These data were consistently analyzed in terms of a trigonal structure containing 21_4 helices. In the following, we shall demonstrate that a 21_4 helical conformation is also consistent with the TEM electron diffraction patterns of oriented PF2/6 on PTFE and we will propose a further insight into the chain packing within the crystal of PF2/6.

In order to ascertain the 21_4 helicity of the PF2/6 chains, we need to determine precisely the position of the first layer line in the ED pattern which allows to determine the helical pitch P with respect to the monomer repeat period p (see Figure 2). The precise relative position of these two reflections can be obtained from the selected area electron diffraction pattern which yields a ratio $P/p = 5.20 \pm 0.06$. Accordingly, there is a clear deviation from the 5:1 ratio expected for a 5_1 or 5_2 helical conformation. A similar result was obtained by Knaapila et al. on shear-oriented PF2/6 samples,[19] indicating that this observation is a general feature of crystalline PF2/6 which depends neither on the substrate used for the orientation nor on the presence of shear during crystallization. The value of P/p is compatible with either a 21_4 or a 26_5 helix. A simple argument based on the intensity of the reflections allows to discard the 26_5 helix. For a 21_4 helix, the strongest reflections are expected to lie on the lth layer lines with $l = 21n \pm 4m$ (n and m are two integers).[35] In the ED pattern of figure 2, we clearly see that the strongest off-meridional reflections are indeed observed on the fourth, 17th, 21st, and 25th layer lines, supporting the 21_4 helicity of PF2/6. A further argument in favor of the 21_4 helix is the fact that this chain conformation is consistent with the 3-fold symmetry of the unit cell as noticed by Knaapila et al.[19] Finally, we would like to mention one important characteristic of the ED pattern in Figure 2, namely the presence on the meridian of two reflections indexed as 0 0 29 and 0 0 58. These reflections have also been observed previously by Knaapila et al. and correspond accordingly to a structural feature specific to crystalline PF2/6. These meridional reflections are not expected in the case of a 21_4 helix. As proposed by Knaapila et al.,[19] we assign these extra reflections to a periodic modulation of the conformation of the ethylhexyl side chains along the helix axis.

3.3.2. Crystal Packing of PF2/6 Chains: A Tentative Model. Most important in the chain conformation determination is the exact value of the monomer repeat period along the chain axis. In the present case, the simultaneous observation of the ED patterns of the PTFE substrate and the oriented PF2/6 films corresponding to the [0 1 0] zone allows for a precise determination of this period which is found to be 0.806 nm ± 0.005 nm. This value is in agreement with the one reported by Knaapila et al. for oriented PF2/6 films on polyimide substrates.[19] The average length of the fluorene monomer obtained from both crystal structure determination.[36] and force field simulations[37] is of about 0.835 nm which is clearly different from the observed period of 0.806 nm along the helix axis of PF2/6. This implies that the monomer long axis must be tilted to the helix axis. From the ratio between these two previous values, we can deduce an average tilt angle of 15 ± 1°.

In a first attempt to verify if the 21_4 helix can be a reasonable solution to reproduce the observed ED patterns, we decided to construct a simplified "mathematical model" which does not take into account the precise chemical structure of the polymer chain. In our structural model, we have used a 21_4 helix made of "atoms" instead of fluorene monomers. The center-to-center distance between successive monomers was fixed to the extended length of the fluorene monomer i.e. 0.835 nm. The first step in the construction of the 21_4 helix was to reproduce the interlayer spacing of 0.806 nm by determining the radius of the 21_4 helix. A value of 0.18 nm was obtained for the radius of the helix.

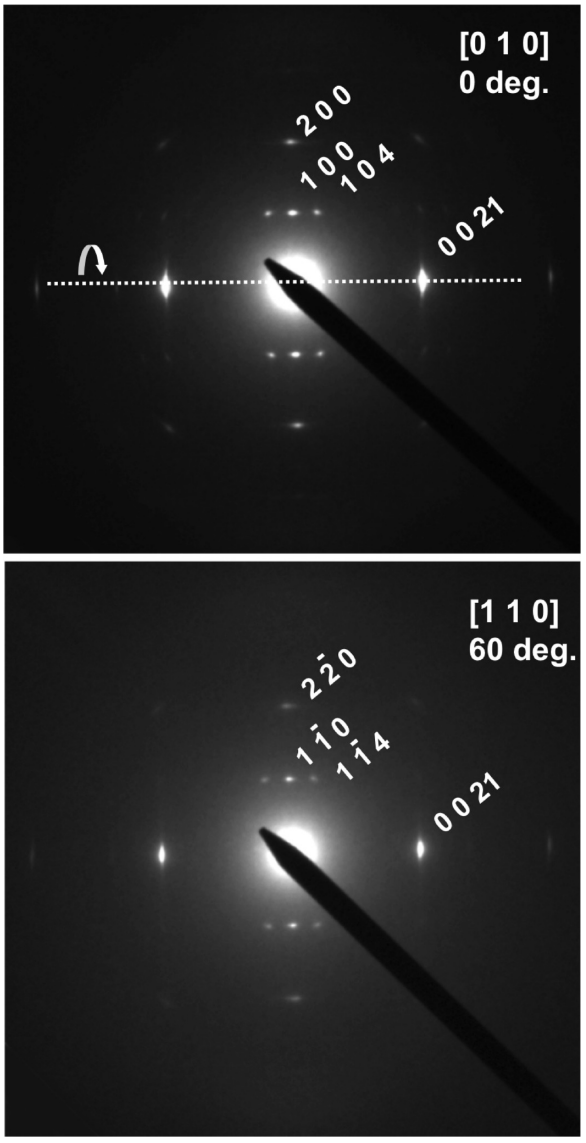

Figure 6. Electron diffraction patterns of an oriented PF2/6 thin film on PTFE substrate corresponding to the [0 1 0] zone and to the [1 1 0] after rotation of the sample by ca. 60° around the chain axis.

In the second step, we have determined the way the three 21_4 helices are packed in a unit cell with $a = b = 1.68$ nm, $c = 16.93$ nm, and $\gamma = 120°$ We first made a rotation−tilt experiment so as to ensure the hexagonal symmetry of the unit cell. A rotation−tilt experiment was performed, tilting the sample around the PF2/6 chain axis $c_{PF2/6}$. As seen in figure 6, upon a rotation of approximately 60° around $c_{PF2/6}$, we obtained an ED pattern rigorously identical to that obtained for 0° rotation. This result indicates that the SAED patterns of the [0 1 0] and the [1 1 0] zones are identical and supports a hexagonal space group. Given the unit cell parameters and the fact that $Z = 3$, the space group has to be chosen as either $P3$, $P3_1$, or $P3_2$.

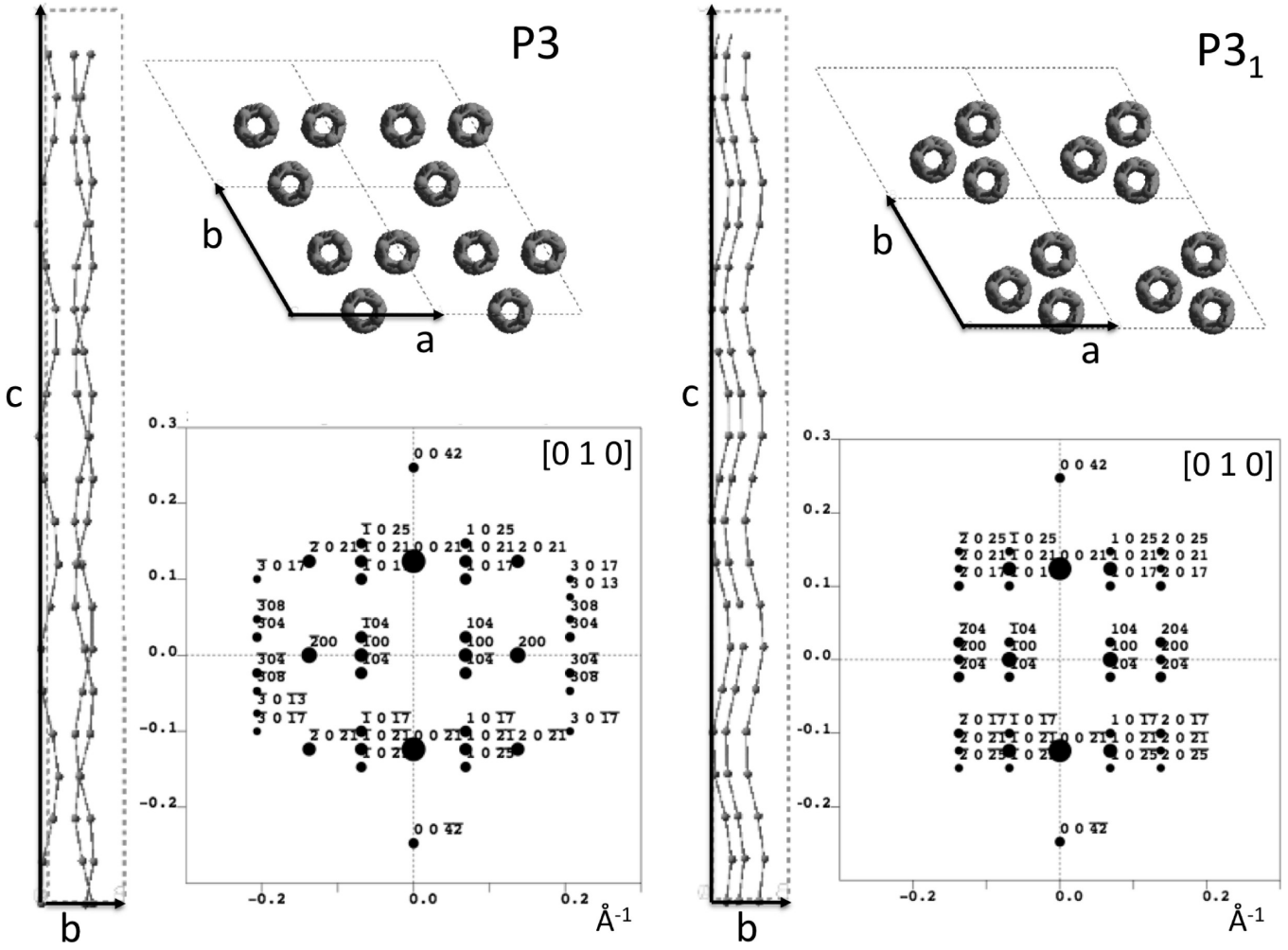

Figure 7. Refined structural models of PF2/6 using a mathematical 21_4 helix, a hexagonal cell and two different space groups ($P3$ and $P3_1$). The figure shows the unit cell projections along the **c**- and **a**-axes and the corresponding calculated ED patterns for the [0 1 0] zone.

For the crystal packing determination, we used a trial-and-error method for each of the space groups. The position and orientation of the 21_4 helices were progressively refined so as to obtain the best agreement between calculated and experimental ED patterns. In particular, the calculated ED patterns have to reproduce the following characteristic features of the experimental pattern: (i) the predominant intensity of the 0 0 21 reflection, (ii) the similar intensities of the {1 0 0} and {1 0 4} reflections, and (iii) the strong 2 0 0 reflection whereas the {2 0 4} reflections are of weak intensity. In Figure 7, we depict the calculated ED patterns yielding the best agreement with the experimental pattern for the $P3$ and $P3_1$ space groups. In the case of the $P3_1$ space group, significant discrepancies are found with respect to the experimental ED pattern: (i) the intensities of the {2 0 4} and the {0 1 21} reflections are clearly overrated and (ii) the intensity of the {1 0 4} and the {2 0 21} are underrated. For the $P3$ space group, a much better agreement is observed; most characteristic features of the experimental ED pattern are observed for the calculated ED pattern (see Figure 7). However, for all three space groups, the refined structure leading to the best agreement with the experimental ED pattern involve a triplet of three PF2/6 chains with relatively short interchain contacts (in the range 0.7−0.8 nm), i.e., the PF2/6 chains are not all strictly equidistant one from another as expected for a true hexagonal packing. Accordingly, this result suggests the existence of peculiar interchain interactions within the triplet of PF2/6 chains.

Let us analyze in more details the refined chain packings obtained for the $P3$ and $P3_1$ space groups. As seen in figure 8, the choice of the $P3_1$ space group results in an interesting situation: the three 21_4 helices keep a constant interchain distance. This situation is similar to that of polyglycine for which three parallel helices are involved in the crystal as proposed by Crick and Rich.[38] In strong contrast to this, for the $P3$ and $P3_2$ space groups, the interchain distance within the triplet of chains shows a periodic oscillation between short and long contacts with a periodicity of approximately five monomer units, leading to a situation similar to that of collagen.[39] At a first glance, it would seem rather logic to choose the $P3_1$ space group in order to minimize the short contacts between the fluorene monomers of the adjacent PF2/6 chains in a triplet. However, our results indicate that the best agreement between the calculated ED pattern and the experimental pattern is obtained when either the $P3$ or the $P3_2$ space groups are used, i.e., when periodic short contacts between monomers are present (see Figure 8). The existence of short contacts might be driven by the possibility of π-stacking between the fluorene monomers every fifth layer whereas the longer contact distances may be due to the ordered packing of the ethylhexyl side chains. Accordingly, the oscillation of the interfluorene distance along the helical axis may reflect a competition between the π stacking of the fluorene monomers (favoring the short contacts) and the efficient crystal packing of the ethylhexyl side chains

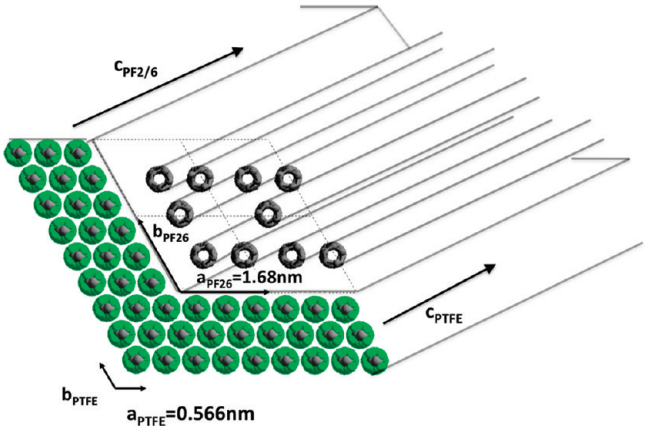

Figure 8. Molecular model of an oriented nucleus of PF2/6 at a PTFE ledge site illustrating the dihedral angle match. The PTFE ledge is represented by the intersection $(1\ 0\ 0)_{PTFE} \cap (0\ 1\ 0)_{PTFE}$. The PF2/6 chains are modeled as 21_4 helices with a radius of 0.18 nm and each monomer is represented by a gray sphere.

(favoring longer interchain distances). This situation reminds the case of the triple helix of collagene.[38] The triple helix of collagene is formed by three left-handed helices that are given a right-handed twist to form a 3-fold superhelix. Such an assembly of chains is essentially stabilized by interchain hydrogen bonding.[38] In the present case, we propose that the supramolecular assembly of the PF2/6 triplet is stabilized by efficient π-stacking between fluorene monomers. Recent spectroscopic results on the formation of the β form of a chiral poly(9,9-bis[(3*S*)-3,7-dimethyloctyl]-2,7-fluorene) seem also to support the possibility for the buildup of some intertwinned helical superstructure.[40] An alternative structural model for PF2/6 might be a superhelix formed by three 5_2 helices (the chain conformation which is most extended) that are given a left-handed twist to form a 3-fold superhelix.

3.4. Origin of the Oriented Growth of PF2/6 vs PFO. Our results have clearly indicated that only PF2/6 chains tend to order in a very efficient manner on the PTFE substrate, not PFO. Let us first consider the possible lattice matches at the polymer/PTFE interface and evaluate the possibility for epitaxy. The high temperature phase of PTFE is described by a pseudohexagonal unit cell with $a = b = 0.566$ nm, $c = 1.95$ nm, $\alpha = \beta = 90°$, and $\gamma = 120°$. The PTFE surface can be modeled by a rectangular cell with $a = 0.566$ nm and $c = 1.95$ nm. However, due to helix reversal defects along c_{PTFE}, the PTFE surface should rather be regarded as a disordered plastic crystalline phase, especially for $T > 50$ °C.[41] For this reason, if epitaxy is responsible of the orientation of PF2/6, it should essentially imply a lattice matching in the direction perpendicular to the PTFE chains (1D epitaxy). The $(1\ 0\ 0)_{PFO}$ contact plane on PTFE is characterized by a rectangular unit cell with $b_{PFO} = 2.34$ nm and $c_{PFO} = 3.24$ nm and for PF2/6 the $(0\ 1\ 0)_{PF2/6}$ contact plane involves a cell with $a_{PF2/6} = 1.68$ nm and $c_{PF2/6} = 16.97$ nm. For both polyfluorenes, interesting conditions of lattice matching can be observed along the a_{PTFE} direction:

$$\text{for PFO: } 4a_{PTFE} = 2.264 \text{ nm vs } b_{PFO} = 2.34 \text{ nm} \quad (3.3\% \text{ mismatch})$$

$$\text{for PF2/6: } 3a_{PTFE} = 1.698 \text{ nm vs } a_{PF2/6} = 1.68 \text{ nm} \quad (1\% \text{ mismatch})$$

This first result indicates a better epitaxial matching condition for PF2/6 than PFO on PTFE. However, the difference in the lattice mismatches may not be sufficiently large to explain the important difference in orientation of PFO and PF2/6 on PTFE. The observation that PF2/6 thin films tend to dewet the PTFE substrate upon annealing suggests that the interaction between the PFs and the PTFE substrate ($E_{PF\text{-}PTFE}$) is certainly lower than the interactions between PF chains, $E_{PF\text{-}PF}$. Accordingly, this situation is similar to that encountered in the case of various conjugated molecular materials oriented on PTFE, e.g., acenes and phthalocyanines. In the case of titanyl phthalocyanine and various acenes, the preferential role of the PTFE ledges on the orientation of the initial seeds was evidenced.[23,24] Preferential nucleation of both pentacene and PcTiO nanodomains was observed at the level of the PTFE ledges (macrosteps).[23,24] In classical models of heterogeneous nucleation at a ledge, the free energy of nucleation of a faceted crystal can be written as follows:[23−25]

$$\Delta G_{nucl} = \sum_{hkl} A_{hkl}\gamma_{hkl} - A_{cs}\gamma_{cs} - \Delta G_c \qquad (1)$$

where A_{hkl}, γ_{hkl} are the areas the surface free energies of the hkl facets. ΔG_c is the free energy associated with the phase change (gas to solid) and cs index refers to the crystal/surface interface.

If the aggregate morphology matches the topography of the ledge, there is a significant reduction of ΔG_{nucl} since $\sum_{hkl} A_{hkl}\gamma_{hkl}$ is lowered at the expense of the interfacial contribution $A_{CS}\gamma_{CS}$. In the case of TiOPc and pentacene, preferential nucleation at PTFE ledges was qualitatively explained by noticing that the PTFE ledge structure matches that of the deposited material at the contact interface. PTFE macrosteps are formed by the intersection of $(1\ 0\ 0)_{PTFE}$ and $(0\ 1\ 0)_{PTFE}$ planes as seen in Figure 7. In the case of PFO, the crystalline domains with orthorhombic structure are oriented with a $(0\ 1\ 0)_{PFO}$ contact plane and with $[0\ 0\ 1]_{PFO}//[0\ 0\ 1]_{PTFE}$. In the case of PF2/6, the domains with a hexagonal structure are oriented with $(0\ 1\ 0)_{PF2/6}//(0\ 1\ 0)_{PTFE}$ and $[0\ 0\ 1]_{PF2/6}//[0\ 0\ 1]_{PTFE}$; i.e., a perfect match can be obtained between the PTFE ledge and the nucleus of PF2/6 since $(1\ 0\ 0)_{PF2/6} \cap (0\ 1\ 0)_{PF2/6} = 120°$ i.e. identical to $(1\ 0\ 0)_{PTFE} \cap (0\ 1\ 0)_{PTFE}$. For PFO, the situation is not as favorable. The most favorable geometrical match between the PTFE ledge and the PFO nucleus, is observed when the $(1\ 2\ 0)_{PFO}$ facet is parallel to $(0\ 1\ 0)_{PTFE}$. However, in this case, $(1\ 2\ 0)_{PFO} \cap (0\ 1\ 0)_{PFO} = 114.6°$, i.e., there is clear mismatch between the PTFE ledge geometry and that of the PFO nucleus. Accordingly, the very high orientation of PF2/6 vs PFO on the PTFE substrate is attributed to the conjunction of (i) a 1D-coincident epitaxy in the direction perpendicular to c_{PTFE} and (ii) a favorable ledge-directed nucleation for PF2/6. Allthough the present analysis is based on the orientation of the crystalline phase of PF2/6 observed at room temperature, it is highly probable that the ledge-directed orientation of PF2/6 is also effective for the "pre-orientation" of the hexagonal liquid crystalline phase above 167 °C.

Beyond the effect of the PTFE ledges on the preferential orientation of the PF2/6 nuclei, it is also worth mentioning the fact that both, PTFE and PF2/6 chains bear a helical structure. PTFE forms a 15_7 helix for $T > 19$ °C whereas PF2/6 forms a 21_4 helix at room temperature (and presumably at higher temperatures). We propose that the preferential orientation of PF2/6 on PTFE may also come from the fact that the PTFE helices trigger the formation of the helical conformation of the PF2/6 chains. An essential issue would be to know if the local chirality of a $(0\ 1\ 0)_{PTFE}$ surface is replicated by the PF2/6 overlayer in terms of handedness of the helices.

4. Conclusion

The growth of oriented polyfluorene thin films on oriented PTFE substrates has uncovered several important structural aspects, especially concerning PF2/6. First, for PF2/6, we have shown that the average lamellar thickness appears to be correlated to the average molecular weight of the polymer: the larger M_n, the larger the average lamellar thickness. Concerning the crystal structure of PF2/6, the ED results strongly support the 21_4 helical conformation of the PF2/6 chains in the crystal, as proposed recently by Knaapila et al.[19] Calculations of the electron diffraction patterns of the [0 1 0] and [1 1 0] zones indicate that the crystal structure of PF2/6 involves a triplet of 21_4 helices in a trigonal cell with space group *P*3. The refined structural model suggests that the supramolecular assembly of the PF2/6 triplet is stabilized by periodic π-stacking between the fluorene monomers of adjacent polymer chains every fifth fluorene monomer.

Acknowledgment. Enlighting discussions with Dr Bernard Lotz are gratefully acknowledged. We are also gratefull to Catherine Foussat and Alain Rameau for performing the SEC measurements. Financial support by the French Ministry of Foreign Affairs through a Hubert Curien project (Nanostructured Interfaces in Electroactive Organic Architectures) is gratefully acknowledged.

Note Added after ASAP Publication. This article was published ASAP on August 25, 2009. Due to a production error, Figures 7 and 8 were inverted. The correct version was published on August 31, 2009.

Supporting Information Available: Figures S1 and S2 show a topographic AFM image and ED pattern of an oreinted PF2/6 thin film on a PTFE substrate. This material is available free of charge via the Internet at http://pubs.acs.org.

References and Notes

(1) Gather, M.; Bradley, D. D. C. *Adv. Funct. Mater.* **2007**, *17*, 479.
(2) Kline, R. J.; McGehee, M. D.; Kadnikova, E. N.; Liu, J.; Fréchet, J. M. J.; Toney, M. F. *Macromolecules* **2005**, *38*, 3319.
(3) Zen, A.; Pflaum, J.; Hirschmann, S.; Zhuang, W.; Jaiser, F.; Asawapirom, U.; Rabe, J. P.; Scherf, U.; Neher, D. *Adv. Funct. Mater.* **2004**, *14*, 757.
(4) Knaapila, M. Winokur, M. J. *Adv. Polym. Sci.* **2008**, *212*, 227−272.
(5) Chen, S.-A., Lu, H.-H. Huang, C.-W. *Adv. Polym. Sci.* **2008**, *212*, 49−84.
(6) Misaki, M.; Ueda, Y.; Nagamatsu, S.; Chikamatsu, M.; Yoshida, Y.; Tanigaki, N.; Yase, K. *Appl. Phys. Lett.* **2005**, *87*, 243503.
(7) Greenham, N. C.; Friend, R. H.; Bradley, D. D. C. *Adv . Mater.* **1994**, *4*, 491.
(8) Rothe, C.; Galbrecht, F.; Scherf, U.; Monkman, A. *Adv. Mater.* **2006**, *18*, 2137.
(9) Grell, M.; Bradley, D. D. C.; Ungar, G.; Hill, J.; Whitehead, K. S. *Macromolecules* **1999**, *32*, 5810.
(10) Winokur, M. J.; Slinker, J.; Huber, D. L. *Phys. Rev. B* **2003**, *67*, 184106.
(11) Chen, S. H.; Chou, H. L.; Su, A. S.; Chen, S. A. *Macromolecules* **2004**, *37*, 6833.
(12) Chen, S. H.; Su, A. C.; Su, C. H.; Chen, S. A. *Macromolecules* **2005**, *38*, 379.
(13) Chen, S. H.; Su, A. C.; Su, C. H.; Chen, S. A. *Macromolecules* **2006**, *39*, 9143.
(14) Chen, S. H.; Su, A. C.; Han, S. R.; Chen, S. A.; Lee, Y. Z. *Macromolecules* **2004**, *37*, 181.
(15) Lieser, G.; Oda, M.; Miteva, T.; Meisel, A.; Nothofer, H.−G.; Scherf, U.; Neher, D. *Macromolecules* **2000**, *33*, 4490.
(16) Grell, M.; Knoll, W.; Lupo, D.; Meisel, A.; Miteva, T.; Neher, D.; Nothofer, H.-G.; Scherf, U.; Yasuda, D. *Adv. Mater.* **1999**, *11*, 671.
(17) Misaki, M.; Ueda, Y.; Nagamatsu, S.; Yoshida, Y.; Tanigaki, N.; Yase, K. *Macromolecules* **2004**, *37*, 6926.
(18) Brinkmann, M. *Macromolecules* **2007**, *40*, 7532.
(19) Knaapila, M.; Torkkeli, M.; Monkman, A. P. *Macromolecules* **2007**, *40*, 3610.
(20) Grell, M.; Bradley, D. D. C.; Inbasekaran, M.; Woo, E. P. *Adv. Mater.* **1997**, *9*, 798.
(21) Wittmann, J.-C.; Smith, P. *Nature* **1991**, *352*, 414.
(22) Lang, P.; Horowitz, G.; Valat, P.; Garnier, F.; Wittmann, J.-C.; Lotz, B. *J. Phys. Chem. B* **1997**, *101*, 8204.
(23) Brinkmann, M.; Graff, S.; Straupé, C.; Wittmann, J.-C.; Chaumont, C.; Nuesch, F.; Aziz, A.; Schaer, M.; Zuppiroli, L. *J. Phys. Chem. B* **2003**, *107*, 10531.
(24) (a) Gearba, R. I.; Anokhin, D. V.; Bondar, A. I.; Bras, W.; Jahr, M.; Lehmann, M.; Ivanov, D. A. *Adv. Mater.* **2007**, *19*, 815. (b) Brinkmann, M.; Wittmann, J.-C.; Barthel, M.; Hanack, M.; Chaumont, C. *Chem. Mater.* **2002**, *14*, 904. (c) Ueda, Y.; Hari, T.; Thumori, T.; Yano, M.; Ni, J. *Appl. Surf.* **1997**, *113*/*114*, 304.
(25) (a) Moulin, J.-F.; Brinkmann, M.; Thierry, A.; Wittmann, J.-C. *Adv. Mater.* **2002**, *14*, 436. (b) Brinkmann, M.; Fite, B.; Pratontep, S.; Chaumont, C. *Chem. Mater.* **2004**, *16*, 4627.
(26) (a) Damman, P.; Zolotukhin, M. G.; Villiers, D.; Geskin, V. M.; Lazzaroni, R. *Macromolecules* **2005**, *35*, 2. (b) Coppée, S.; Geskin, V. M.; Lazzaroni, R.; Damman, P. *Macromolecules* **2004**, *37*, 244.
(27) (a) Ueda, Y.; Kuriyama, T.; Hari, T.; Ashida, M. *J. Electron Microsc.* **1994**, *43*, 99. (b) Moggio, I.; Le Moigne, J.; Arias-Marin, E.; Issautier, D.; Thierry, A.; Comoretto, D.; Dellepiane, G.; Cuniberti, C. *Macromolecules* **2001**, *34*, 7091.
(28) Knaapila, M.; Lyons, B. P.; Kisko, K.; Foreman, J. P.; Vainio, U.; Mihaylova, M.; Seeck, O. H.; Pålsson, L.-O.; Serimaa, R.; Torkkeli, M.; Monkman, A. P. *J. Phys. Chem. B* **2003**, *107*, 12425.
(29) Miyaura, K.; Suzuki, A. *Chem. Rev.* **1995**, *95*, 2457.
(30) Scherf, U.; List, E. J. W. *Adv. Mater.* **2002**, *14*, 477.
(31) Brinkmann, M.; Wittmann, J.-C. *Adv. Mater.* **2006**, *18*, 860.
(32) (a) Brinkmann, M.; Rannou, P. *Adv. Funct. Mater.* **2007**, *17*, 101. (b) Brinkmann, M.; Rannou, P. *Macromolecules* **2009**, *42*, 1125.
(33) Blondin, P.; Bouchard, J.; Beaupré, S.; Belletête, M.; Durocher, G.; Leclerc, M. *Macromolecules* **2000**, *33*, 5874.
(34) Tanto, B.; Gusha, S.; Martin, C. M.; Scherf, U.; Winokur, M. J. *Macromolecules* **2004**, *37*, 9438.
(35) Cochran, W.; Crick, F. H.; Vand, V. *Acta Crystallogr.* **1952**, *5*, 581.
(36) Destri, S.; Pasini, M.; Botta, C.; Porzio, W.; Bertini, F.; Marchiò, L. *J. Mater. Chem.* **2002**, *12*, 924.
(37) Grell, M.; Bradley, D. D. C.; Long, X.; Chamberlain, T.; Inbasekaran, M.; Woo, E. P.; Solimann, M. *Acta Polym.* **1998**, *49*, 439.
(38) Crick, F. H. C.; Rich, A. *Nature* **1955**, *176*, 780.
(39) Dickerson, R. E.; Geis, I. *The structure and action of proteins*; Harper and Row: New York.
(40) Lakhwani, G.; Meskers, S. C. J. *Macromolecules* **2009**, *42*, 4220.
(41) Kimmig, M.; Strobl, G.; Stuhn, B. *Macromolecules* **1994**, *27*, 2481.